



Submitted to

32nd International Conference on High Energy Physics, ICHEP04, August 16, 2004, Beijing

Abstract: **6-0183**

Parallel Session **6**

www-h1.desy.de/h1/www/publications/conf/conf_list.html

Diffractive photoproduction of high- p_t photons at HERA

H1 Collaboration

Abstract

The process $\gamma p \rightarrow \gamma Y$ in which the outgoing photon has transverse momentum $p_{t(\gamma)} > 2$ GeV and there is a large rapidity gap between the proton dissociative system Y and the outgoing photon is studied for the first time with the H1 detector at HERA. Cross sections are measured differentially in the squared 4-momentum transfer at the proton vertex, t , and $x_p = (E + p_z)_\gamma / 2E_p$, where E_p is the incoming proton energy. All cross sections are consistent with a perturbative QCD model calculated using the leading logarithmic approximation of BFKL.

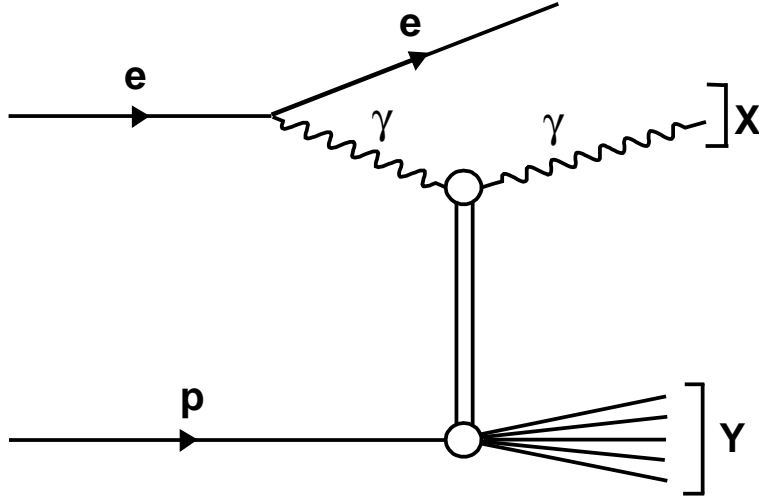


Figure 1: Schematic illustration of the process $\gamma p \rightarrow \gamma Y$.

1 Introduction

The process $\gamma p \rightarrow \gamma Y$ (figure 1) where the final state photon carries a large transverse momentum and is well separated from the proton dissociative system Y provides a uniquely clean probe of the underlying dynamics of the diffractive process [1–5]. Requiring that the scattered photon has a large transverse momentum $p_{t(\gamma)}^2 \simeq -t \gg \Lambda_{\text{QCD}}^2$ ensures the applicability of perturbative QCD [6]. Because the X system consists of only a single photon, an experimental measurement can be made in an extended pseudorapidity range compared with high- t diffractive vector meson production [7, 8]. This has the important effect of giving access to the region of large centre of mass energy of the hard subprocess \hat{s} (the separation in rapidity between the struck parton in the proton and the final state photon is $\Delta\eta \simeq \log(\hat{s}/p_{t(\gamma)}^2)$), which is desirable from a theoretical point of view because perturbative calculations within the leading logarithmic approximation of BFKL [9–11] are strictly valid only in the asymptotically high \hat{s} region. The theoretical calculations are further simplified by the absence of a vector meson wavefunction: the only non-perturbative part resides within the proton structure function, which factorises in the usual way.

After a brief description of the H1 detector in section 2, the selection of the events and the definitions of the measured cross sections are discussed in section 3. The Monte Carlo models used to correct the data and to compare to the BFKL predictions, are described in 4. The results and model comparisons are presented and discussed in section 5.

2 The H1 Detector

A detailed description of the H1 apparatus can be found elsewhere [12]. The following briefly describes the detector components relevant to this analysis.

A liquid argon (LAr) calorimeter covers the range in polar angle $4^\circ < \theta < 153^\circ$ ($3.35 > \eta > -1.43$) with full azimuthal coverage¹. The LAr calorimeter consists of an electromagnetic section with lead absorbers and a hadronic section with steel absorbers, with a combined depth between 4.5 and 8 interaction lengths. Both sections are highly segmented in the transverse and longitudinal directions with about 44000 cells in total. The absolute hadronic energy scale is known to 4% for this analysis. The polar region $153^\circ < \theta < 177.8^\circ$ ($-1.43 > \eta > -3.95$) is covered by the SPACAL [13], a lead-scintillating fibre calorimeter with both electromagnetic and hadronic sections, with a combined depth of 2 interaction lengths. The scattered photon energy is measured in this detector to an accuracy of 1%. The scattered photon angle is measured to an accuracy of ± 1 mrad.

Charged particles are detected in the Central Tracking Detector (CTD) ($1.74 > \eta > -1.74$) and Backward Silicon Tracker (BST) ($-1.84 > \eta > -3.35$). The CTD comprises two large cylindrical jet drift chambers and two z -chambers arranged concentrically around the beam-line. The BST consists of eight planes of silicon detector discs with 16 wedge shaped four-inch wafers per disc. The trackers lie within a solenoidal magnetic field of 1.15T.

The luminosity is measured from the reaction $ep \rightarrow ep\gamma$ with two TlCl/TlBr crystal calorimeters [12], the electron and photon taggers, installed in the HERA tunnel. The electron tagger is located at $z = -33$ m from the interaction point in the direction of the outgoing lepton beam and the photon tagger is at $z = -103$ m.

3 Event Selection and Kinematic Reconstruction

The data for this analysis were collected with the H1 detector during the 1999-2000 running period, when HERA collided 27.6 GeV positrons with 920 GeV protons. An integrated luminosity of 47.6 pb^{-1} is used.

Photoproduction events were selected by detecting the scattered positron in the electron tagger of the luminosity system. This restricts the virtuality of the photon to $Q^2 < 0.01 \text{ GeV}^2$. The photon-proton centre of mass energy was restricted to the range $175 < W < 247 \text{ GeV}$ to avoid regions of low electron tagger acceptance.

Events were triggered by demanding energy in the electromagnetic section of the SPACAL calorimeter. One of the triggers used additionally required an energy deposit in the 33m electron tagger. No tracking requirements were imposed at the trigger level. The trigger efficiency was calculated from data using a combination of independent triggers and special data-taking runs, and found to be close to 100 % for all measured data points.

Photons with an energy of at least 8 GeV were identified in the SPACAL calorimeter by imposing cuts on the electromagnetic cluster radius and hadronic energy behind the cluster, and demanding that there was no track associated with the cluster. Additional fiducial cuts were applied on the position of the cluster in SPACAL to remove regions of low efficiency. No other energy deposits (above a noise threshold) were allowed in the SPACAL.

¹ θ is measured relative to the outgoing proton beam direction, which defines the positive z axis and the forward direction. Pseudorapidity is defined as $\eta = -\ln(\tan\theta/2)$.

Hadronic final state objects were defined using a combination of tracking and calorimetric information. An algorithm was used which avoids the double counting of tracks and calorimeter clusters [14].

Diffractive events were selected by requiring that $y_{\mathcal{P}} < 0.018$, where

$$y_{\mathcal{P}} = \frac{p \cdot (q - X)}{q \cdot p} \simeq \frac{\sum_Y (E - P_z)}{2E_\gamma}. \quad (1)$$

Here, p and q are the 4-vectors of the incoming proton and photon respectively and X is the 4-vector of the scattered photon. The quantity is calculated experimentally by summing the $E - P_z$ of all hadronic final state objects in the event (i.e. all measured particles except the scattered electron and high p_t photon), and dividing by twice the incoming photon energy E_γ . This method has the experimental advantage that particles lost in the forward beam pipe do not contribute much to the numerator. As $y_{\mathcal{P}} \simeq e^{-\Delta\eta}$, this cut ensures that there is a large rapidity gap between the photon and the proton dissociative system². However, no proton dissociative system is required to be seen in the detector.

In addition to the kinematic variables defined above, the variable $x_{\mathcal{P}}$ is defined as

$$x_{\mathcal{P}} = \frac{q \cdot (p - Y)}{q \cdot p} \simeq \frac{(E + P_z)_\gamma}{2E_p}, \quad (2)$$

where Y is the 4-vector of the proton dissociative system, $(E + P_z)_\gamma$ is the $E + P_z$ of the photon candidate and E_p is the energy of the incident proton.

4 Monte Carlo simulations and data corrections

The HERWIG 6.1 [15] Monte Carlo event generator was used to correct the data for detector acceptance and bin migration effects, and to make model comparisons. HERWIG is the only event generator at present in which the diffractive high- t photon sub-process has been implemented. Details can be found in [5]. The calculation has been completed within the leading logarithmic approximation (LLA) of BFKL, and includes contributions from both real and virtual incoming photons [3, 4]. At leading logarithmic accuracy, the strong coupling constant α_s is a fixed parameter. This means that there are two independent free parameters in the calculation: the value of α_s in the pre-factor of the cross section (which enters to the fourth power) and the value of α_s in the pomeron intercept $1 + \omega_0$, where $\omega_0 = (3\alpha_s/\pi)4\ln 2$ in the LLA. In all that follows, we chose these two values of α_s to be equal (α_s will henceforth be referred to as $\overline{\alpha_s}$). Note, however, that this is an arbitrary choice. In particular, to the accuracy of the present calculations

$$\frac{d\sigma}{dx_{\mathcal{P}}} \sim \frac{1}{W^2} \left(\frac{1}{x_{\mathcal{P}}} \right)^{2\omega_0+2}, \quad (3)$$

so the slope of the $x_{\mathcal{P}}$ distribution is affected only by the choice of $\overline{\alpha_s}$ in the pomeron intercept.

²To ensure efficient background rejection, a minimum rapidity gap of $\Delta\eta = 2$ is required between the photon candidate and the edge of the proton dissociative system. This requirement is corrected for in the final cross sections.

A HERWIG sample with $\overline{\alpha_s} = 0.17$ was passed through a full simulation of the H1 detector and used to correct the data for detector acceptance and bin migration effects. This sample was found to give a good description of the data for all kinematic distributions considered. In order to investigate the model dependence of the detector correction procedure, the Monte Carlo sample was reweighted in $x_{\mathbb{P}}$, $p_{t(\gamma)}$ and M_Y , the mass of the proton dissociative system. The model dependence of the detector acceptance corrections was included in the systematic errors as detailed in section 5.

The photon-proton (γp) cross sections were extracted by dividing the ep cross sections by the effective photon flux [17] integrated over the W and Q^2 range of the measurement.

The background from inclusive diffractive photoproduction events, in which a single electromagnetic particle fakes the photon candidate in the SPACAL or escapes detection, and all other hadronic activity falls below the SPACAL noise cuts, was simulated using the PHOJET Monte Carlo generator [16]. There was a small contamination from this background of less than 9% for all bins. A bin-by-bin subtraction was made to remove this background. In order to investigate the background from high- t diffractive ω production, where the ω decays in the $\pi^0\gamma$ channel, a sample was generated using the DIFFVM Monte Carlo [18]. The contribution was found to be negligible. Background from standard DIS events, in which the scattered electron fakes the photon candidate and an overlapping photoproduction or Bethe-Heitler event produces an electron in the 33m tagger, was also considered and found to be negligible.

5 Results and Discussion

The γp cross section differential in $x_{\mathbb{P}}$, in the range $175 < W < 247$ GeV, $p_{t(\gamma)} > 2$ GeV, $y_{\mathbb{P}} < 0.018$, is shown in figure 2. The cross section is defined at the level of stable hadrons. The inner error bars show the statistical error and the outer error bars show the statistical and systematic errors added in quadrature. The largest systematic error is due to the error in the noise subtracted from the LAr calorimeter. The total systematic uncertainty is small compared to the statistical error. Also shown are the LLA BFKL predictions from the HERWIG Monte Carlo. As described in section 4, the data are sensitive to the choice of the $\overline{\alpha_s}$ parameter in the prediction in two ways. The first is the slope of the $x_{\mathbb{P}}$ distribution which, as equation 2 shows, is related to the BFKL pomeron intercept. The cross section clearly rises steeply as $x_{\mathbb{P}}$ becomes small - the classic signature of a diffractive process. Within the errors, it is difficult to distinguish between the slopes of the 3 choices of $\overline{\alpha_s}$, although perhaps $\overline{\alpha_s} = 0.15$ (a pomeron intercept of ~ 1.4) leads to too shallow a rise with $1/x_{\mathbb{P}}$. The second point of interest is the normalisation of the cross section predictions. Here, a choice of $\overline{\alpha_s} = 0.17$ gives too large a cross section. It should be noted however that there is some normalisation uncertainty within the LLA, even given a choice of $\overline{\alpha_s}$. It may therefore be possible to fix both $\overline{\alpha_s}$ values at 0.17 and obtain a good description of the data in both normalisation and shape. This is in comparison to the value $\overline{\alpha_s} = 0.18$ as used for recent H1 measurements [8, 19].

The γp cross section differential in the squared 4-momentum transfer t between proton and the incoming photon (where in photoproduction $-t \sim p_{t(\gamma)}^2$), in the range $175 < W < 247$ GeV, $0.0001 < x_{\mathbb{P}} < 0.0007$, $y_{\mathbb{P}} < 0.018$, is shown in figure 3. The largest systematic error is due to the error in the noise subtracted from the LAr calorimeter. The total systematic uncertainty

is small compared to the statistical error. In this case, the agreement in the shape of the cross section between the HERWIG predictions and the data is perhaps more questionable, for all values of $\overline{\alpha_s}$ chosen here.

It is worth bearing in mind that there may be important contributions from higher order effects beyond the LLA, so strong statements about the agreement with the LLA may be premature. This said, however, the fact that the measured cross section exhibits such a dramatic rise with energy is a striking result, and there is an reasonable overall agreement with the LLA BFKL predictions.

6 Conclusions

The process $\gamma p \rightarrow \gamma Y$ where the photon carries a large transverse momentum and is well separated from the proton dissociative system Y has been studied. Cross sections have been measured differentially in the appropriate energy variable $x_{\mathbb{P}}$ and the squared 4-momentum transfer at the proton vertex, t . The cross sections are found to be in reasonable agreement in both normalisation and shape with the predictions of the leading logarithmic approximation of BFKL. In particular, the cross section is found to rise very steeply with decreasing $x_{\mathbb{P}}$.

Acknowledgements

We thank Jeff Forshaw for many useful discussions and suggestions. We are grateful to the HERA machine group whose outstanding efforts have made and continue to make this experiment possible. We thank the engineers and technicians for their work in constructing and now maintaining the H1 detector, our funding agencies for financial support, the DESY technical staff for continual assistance, and the DESY directorate for the hospitality which they extend to the non DESY members of the collaboration.

References

- [1] I. F. Ginzburg, S. L. Panfil and V. G. Serbo, Nucl. Phys. B **284** (1987) 685.
- [2] I. F. Ginzburg and D. Y. Ivanov, Phys. Rev. D **54** (1996) 5523 [hep-ph/9604437].
- [3] D. Y. Ivanov and M. Wusthoff, Eur. Phys. J. C **8** (1999) 107 [hep-ph/9808455].
- [4] N. G. Evanson and J. R. Forshaw, Phys. Rev. D **60** (1999) 034016 [hep-ph/9902481].
- [5] B. E. Cox and J. R. Forshaw, J. Phys. G **26** (2000) 702 [hep-ph/9912486].
- [6] J. R. Forshaw and P. J. Sutton, Eur. Phys. J. C **1** (1998) 285. [hep-ph/9703225].
- [7] S. Chekanov *et al.* [ZEUS Collaboration], Eur. Phys. J. C **26** (2003) 389 [hep-ex/0205081].

- [8] A. Aktas *et al.* [H1 Collaboration], DESY-03-061
- [9] E. A. Kuraev, L. N. Lipatov and V. S. Fadin, Sov. Phys. JETP **45** (1977) 199 (Zh. Eksp. Teor. Fiz. **72** (1977) 377).
- [10] I. I. Balitsky and L. N. Lipatov, Sov. J. Nucl. Phys. **28** (1978) 822. (Yad. Fiz. **28** (1978) 1597).
- [11] L. N. Lipatov, Sov. Phys. JETP **63** (1986) 904. (Zh. Eksp. Teor. Fiz. **90** (1986) 1536).
- [12] I. Abt *et al.* [H1 Collaboration], Nucl. Instrum. Meth. A **386** (1997) 310 and 348.
- [13] H1 SPACAL group, R.D. Appuhn *et al.*, Nucl. Instr. and Meth. **A386** (1997) 397.
- [14] C. Adloff *et al.* [H1 Collaboration], Z. Phys. C **74** (1997) 221.
- [15] G. Marchesini, B. R. Webber, G. Abbiendi, I. G. Knowles, M. H. Seymour and L. Stanco, Comput. Phys. Commun. **67** (1992) 465.
- [16] F. W. Bopp, R. Engel and J. Ranft, hep-ph/9803437.
- [17] C. Weizsacker, Z. Phys **88** (1934) 612.
E. Williams, Phys. Rev. **45** (1934) 729.
- [18] B. List and A. Mastroberardino, “Workshop on Monte Carlo Generators for HERA Physics”, Hamburg, Germany, 27-30 April 1998.
- [19] C. Adloff *et al.* [H1 Collaboration], Eur. Phys. J. C **24** (2002) 517 [hep-ex/0203011].

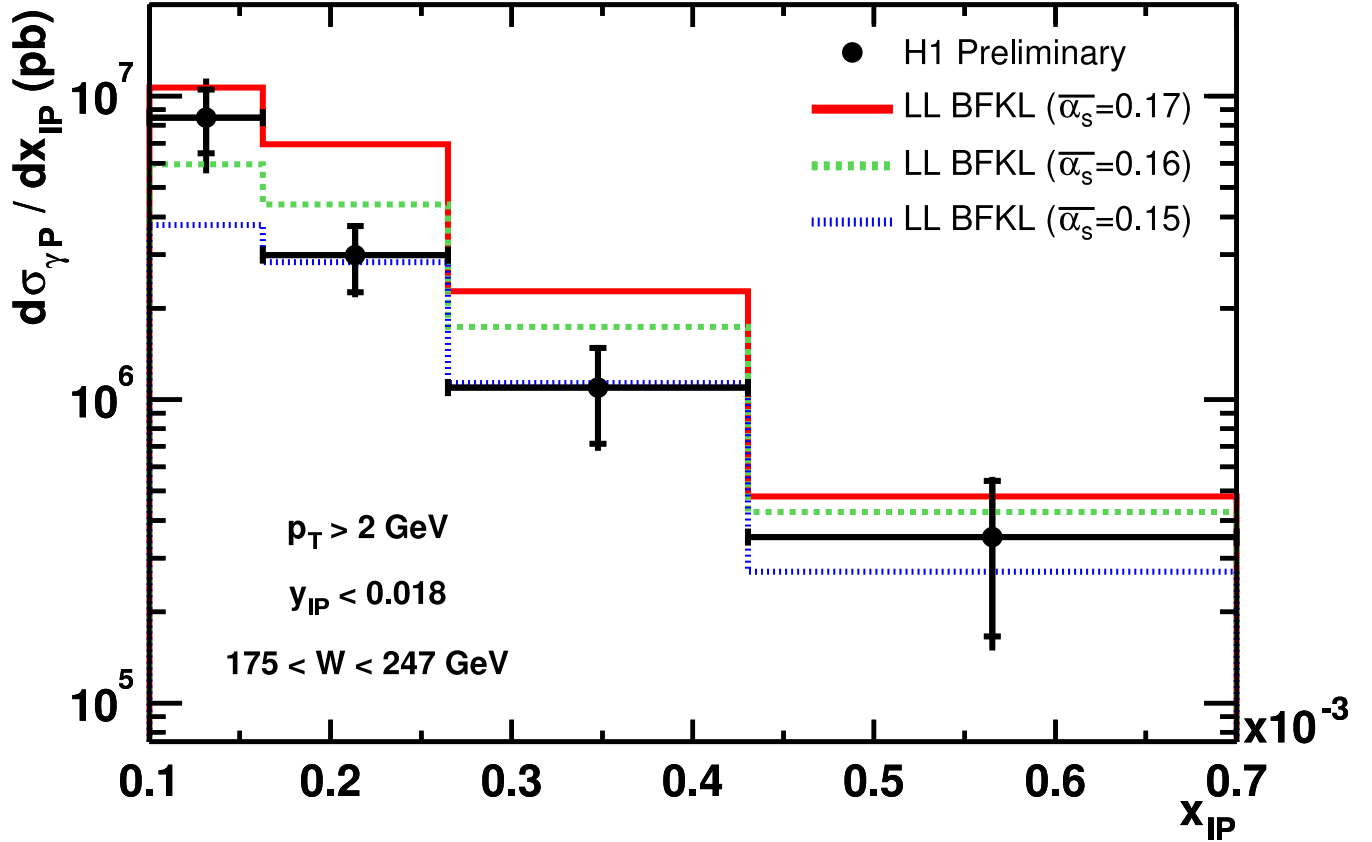


Figure 2: The γp cross section differential in x_{IP} . The inner error bars show the statistical error and the outer error bars show the statistical and systematic errors added in quadrature. The dotted line shows the prediction of the leading logarithmic approximation of BFKL as implemented in HERWIG, for the choice of fixed $\bar{\alpha}_s = 0.15$ in the prefactor and pomeron intercept, as described in the text. The dashed line and solid line show the same calculation, for $\bar{\alpha}_s = 0.16$ and $\bar{\alpha}_s = 0.17$ respectively.

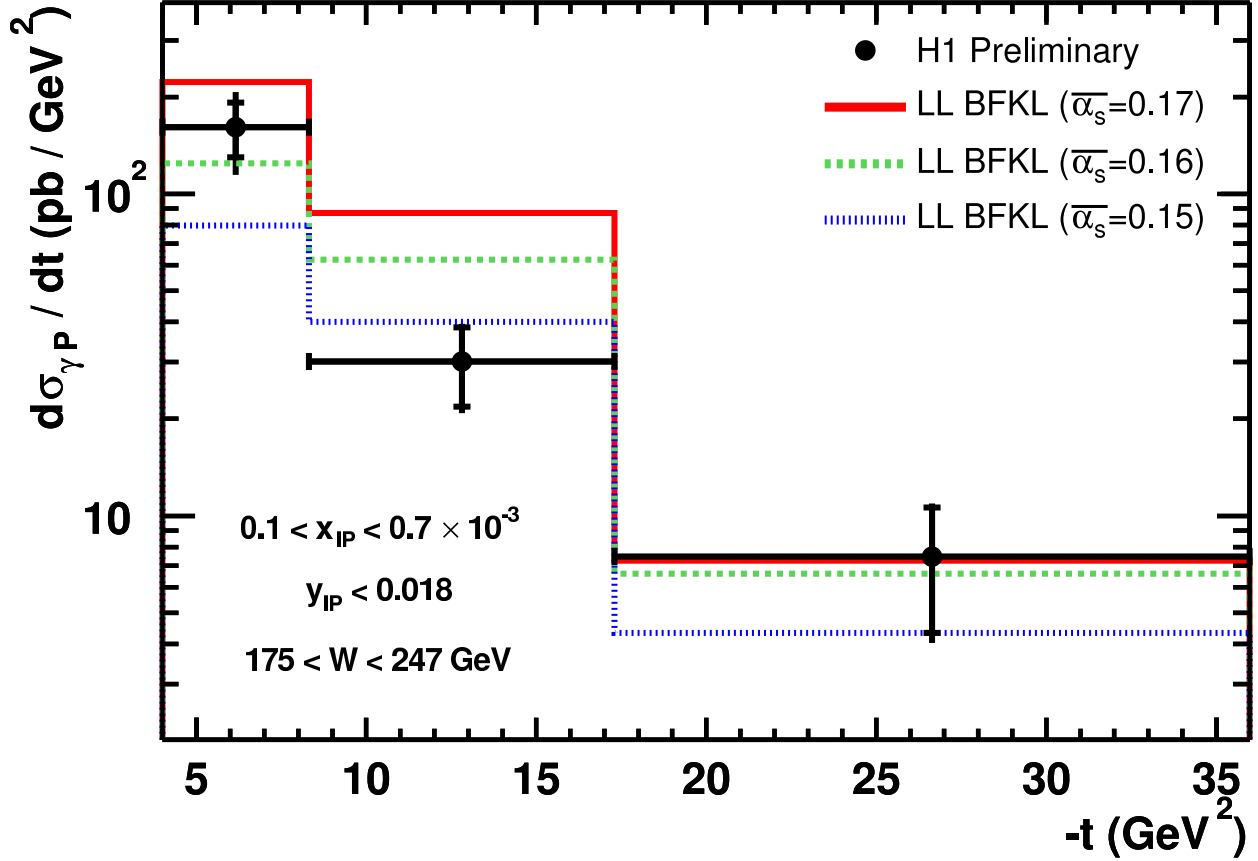


Figure 3: The γp cross section differential in the squared 4-momentum transfer t at the proton vertex. The inner error bars show the statistical error and the outer error bars show the statistical and systematic errors added in quadrature. The dotted line shows the prediction of the leading logarithmic approximation of BFKL as implemented in HERWIG, for the choice of fixed $\bar{\alpha}_s = 0.15$ in the prefactor and pomeron intercept, as described in the text. The dashed line and solid line show the same calculation, for $\bar{\alpha}_s = 0.16$ and $\bar{\alpha}_s = 0.17$ respectively.